MOLECULAR DYNAMICS COMPUTATION OF GAS-PHASE NANOPARTICLE SINTERING: A COMPARISON WITH PHENOMENOLOGICAL MODELS

Michael R. Zachariah* and Michael J. Carrier

Chemical Science and Technology Laboratory, National Institute of Standards and Technology, Gaithersburg, MD 20899, U.S.A.

Abstract—The mechanism and kinetics of the growth of silicon nanoparticles via particle–particle interactions has been investigated through the use of classical molecular dynamics (MD) trajectory calculations. Computations over a broad range of temperatures and particle sizes have shown that particle sintering is very dependent on size and temperature when solid-like, and considerably less sensitive when liquid-like. These atomistic computations have been used for the first time to validate previously postulated phenomenological mechanisms/models for both solid and liquid particle coalescence. The results have shown that solid-like particles sinter by a solid-state diffusion mechanism while liquid-like particles sinter by a viscous flow mechanism. © 1999 Elsevier Science Ltd. All rights reserved

1. INTRODUCTION

One of the major obstacles to the widespread use of nanoscale materials is the difficulty in producing fine particles with the desired chemical purity, phase and morphology. These challenges are greatly exacerbated by the need to produce these materials in both large quantities and at a sufficiently low cost. The conventional wisdom is that in order to satisfy these two requirements, a vapor-phase process is the synthesis method of choice. Unfortunately, vapor-phase growth processes have the propensity to form agglomerated rather than spherical particles. This occurs when the characteristic sintering (coalescence) time is greater than the characteristic time for particle–particle collisions (Siegel, 1994). While considerable attention has been paid to the development of phenomenological sintering models (German, 1996), little attention thus far has been directed from a fundamental molecular level. The importance of the size-dependent properties of nanoparticles have been recently reviewed by Preining (1998), who very clearly outlines the need to understand properties from a molecular viewpoint. There have been a few recent studies that have focused on the sintering of nanoparticles from an atomistic view. In two recent publications, Zhu and Averback looked at the sintering of copper nanoparticles (Zhu and Averback, 1996a, b). Other studies have included an investigation by Blaisten-Barojas and Zachariah (1992) on silicon cluster–cluster collision processes for particles up to 30 atoms and some earlier work by Gay and Berne (1986) on the collision of Lennard–Jones particles.

In a recent paper, we looked in detail at the equilibrium properties of small silicon particles (Zachariah *et al.*, 1996) and now extend these results by focusing attention on the kinetic and dynamical aspects of nanoparticle growth. The goal of this work was to develop a sufficiently robust set of data and principles to define the important mechanistic aspects of nanoparticle sintering. The results of these computations are used here for the first time to define and validate phenomenological models for particle growth.

* Author to whom correspondence should be addressed at: University of Minnesota, E-mail: mrz@me.umn.edu.

2. COMPUTATIONAL METHOD

Simulations were conducted by classical molecular dynamics (MD) methods as described in our previous studies (Zachariah *et al.*, 1994, 1996a) of silicon nanoparticles using the three-body interatomic potential developed by Stillinger and Weber (SW) (1985). This empirical potential contains two- and three-body interactions which take into consideration the directional characteristic of the covalent bonding and are given in equations (1a)–(1c).

$$v = \sum_{\substack{i,j \\ i<j}} v_2(i,j) + \sum_{\substack{i,j,k \\ i<j<k}} v_3(i,j,k). \tag{1a}$$

Two-body term:

$$v_2(r) = \begin{cases} A(Br^{-p} - r^{-q})e^{-1/(r-a)}, & r < a, \\ 0, & r \geqslant a. \end{cases} \tag{1b}$$

Three-body term:

$$v_3(\mathbf{r}_i, \mathbf{r}_j, \mathbf{r}_k) = h(r_{ij}, r_{ik}, \theta_{jik}) + h(r_{ji}, r_{jk}, \theta_{ijk}) + h(r_{ki}, r_{kj}, \theta_{ikj}), \tag{1c}$$

$$h(r_{ij}, r_{ik}, \theta_{jik}) = \lambda e^{\gamma/(r_{ij}-a) + \gamma/(r_{ik}-a)}(\cos\theta_{jik} + \tfrac{1}{3})^2,$$

where r is the distance between a pair of atoms, a is the cutoff distance of the two-body potential, and θ_{ijk} is the bond angle between a triplet of atoms. The parameters (A, B, p, q, λ, γ) are constants formulated by Stillinger and Weber (1985) and are specific to liquid silicon. Molecular dynamics methods are in many ways an ideal tool for studies of these systems because of their finite size. Ultimately, all transport and thermophysical properties are based on atomic interactions/reactions, which MD methods are ideally suited to probe. Particle morphology changes also require the movement of atoms by either bulk fluid motion or by atomic diffusion, both of which can be studied by atomistic molecular dynamic methods. Ideally, the results from MD computations should lead to the determination of property data as well as phenomenological mechanisms. Unfortunately, the very nature of molecular dynamics, which focuses on individual atomic motion, makes it difficult to define phenomenological mechanisms due to this atomistic viewpoint.

An alternative approach is to postulate a phenomenological model and use MD to obtain the fundamental constants (diffusion constants, viscosity, surface tension, etc.) which are used in the model to keep it self-consistent. We then conduct MD simulations of the phenomena of interest (e.g. sintering) and assess the quality of the comparison. Essentially, one uses the MD simulation as both the experiment and the theory. This is the approach taken in this paper.

The simulations were conducted in *three stages*:

1. *Particle equilibration*: Particle configurations of 30, 60, 120, 240 and 480 atoms were generated. The first step in the equilibration process was to remove any angular momentum from the particle. The particle was then set to the desired temperature using constant temperature molecular dynamics for a period of 50 ps. At the end of this time segment the simulation was switched to a constant energy calculation for 20 ps, and the temperature was recorded over that interval. If the average temperature of the particle deviated by less than 10 K over this period, the equilibration was considered a success. If not, then the process was repeated. Particles at 600, 750, 900, 1200, 1600 and 2000 K were generated for each particle size.

2. *Particle property simulation*: Following equilibration, particle properties were averaged using constant energy molecular dynamics over a period of 25 ps.

3. *Particle–particle collisions*: Replicate particles were generated and then collided with zero impact parameter and with collision energies equivalent to the internal temperature of

the particles in order to simulate thermal collisions. The morphology was tracked to full coalescence.

3. PARTICLE STRUCTURE AND PROPERTIES

The properties of the particles used for these sintering studies have been extensively reviewed in a prior publication (Zachariah *et al.*, 1996a). We briefly summarize those results. Equilibrated solid particles were found to have an interior structure (e.g. inner 60 atoms of a 480-atom cluster) most closely related to a "glassy" or supercooled liquid. These results are expected since the SW potential is known for its inability to quench the liquid to an amorphous state. The resulting bonding structure of the "glassy" particle is about 50% five-coordinated while a silicon crystal is four-coordinate. The liquid droplets showed coordination numbers of about 8.5, in agreement with bulk SW calculations. The coordination number for surface atoms for the solid particles were about 80% three-coordinate with the remaining four-coordinated. In general, the average coordination number increased slowly with temperature, except for the inner atoms which had a sharp increase in coordination number at the melting point. Vibrational structure was found to be qualitatively similar to the phonon density of states for bulk silicon.

4. PARTICLE COALESCENCE KINETICS

The rate of particle coalescence has a significant impact on the final morphology observed. The temporal evolution of nanoparticle growth in a gas-phase process is depicted schematically in Fig. 1. This process often results in chained agglomerates of small particles (Fig. 2a), while the desirable morphologies are spherical or soft agglomerates, which may also contain a second component that has formed by intraparticle coalescence (Fig. 2b). Since coalescence (sintering) processes are generally occurring simultaneously or subsequent to nucleation, the ability to predict the time scales and basic physics behind sintering of nanoparticles could be very useful in the construction of aerosol models that account for particle shapes (Koch and Friedlander, 1990). In fact, aerosol researchers who are interested in materials processing often direct much of their effort towards minimizing agglomeration (Xiong *et al.*, 1993; Girshick *et al.*, 1995). The essence of the problem involves a competition between the time for particle–particle collisions and the rate of particle coalescence. If the collision time is long relative to the characteristic sintering (coalescence) time, we will grow spherical particles, since on average a particle doublet will have coalesced

GAS PHASE PARTICLE GROWTH

$\tau_{sintering} < \tau_{collision}$

SPHERICAL

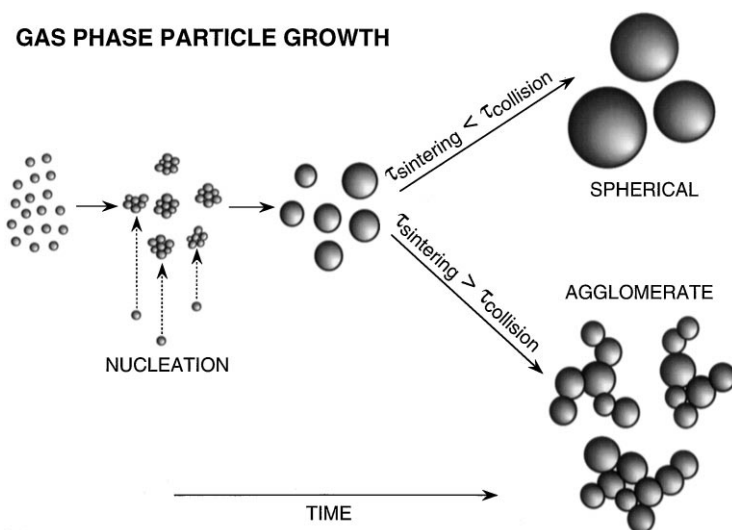$\tau_{sintering} > \tau_{collision}$

AGGLOMERATE

NUCLEATION

TIME

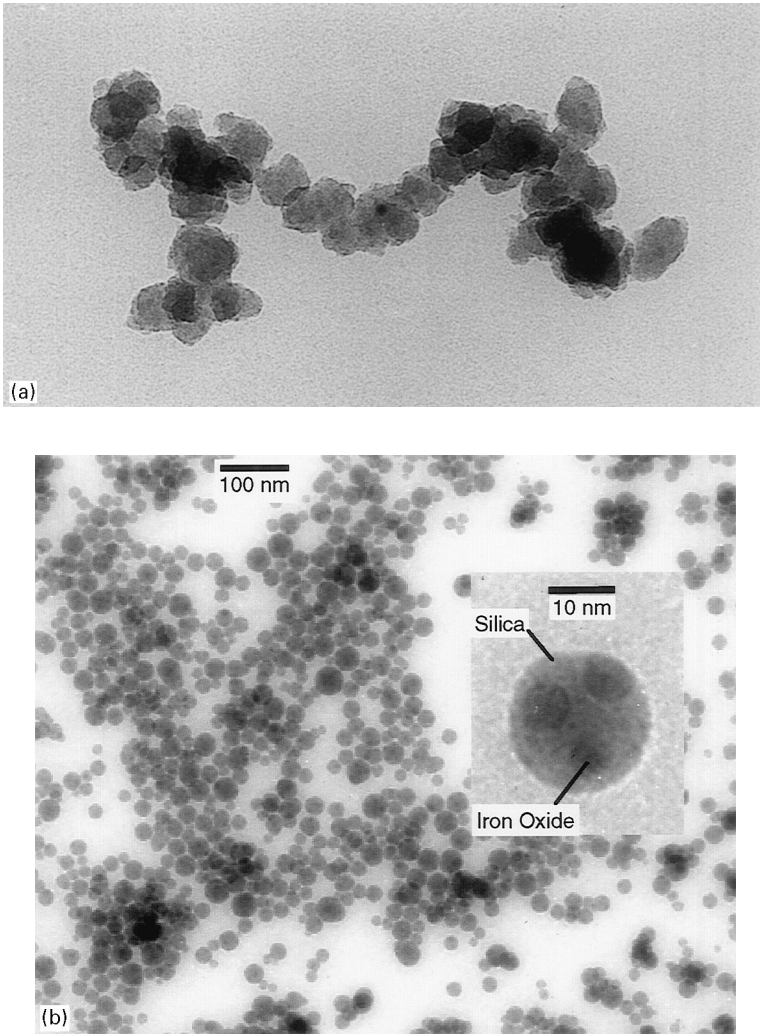Fig. 1. Temporal evolution of vapor-phase particle growth.

Fig. 2. Examples of agglomerates and spherical nanoparticles formed from vapor phase growth. (a) agglomerate of SiO_2, (b) spherical superparamagnetic nanocomposite of SiO_2/γ-Fe_2O_3 (Zachariah et al., 1996b).

before another particle encounter. If however, as is so often the case, collisions between particles occur faster than coalescence, chain aggregates similar in morphology to that formed in sooting flames are produced.

$$\tau_{sintering} < \tau_{collision} \Rightarrow \text{Spherical particle,}$$

$$\tau_{sintering} > \tau_{collision} \Rightarrow \text{Agglomerate.}$$

Naturally, both number concentration and temperature are important variables in defining characteristic times for collision and sintering, respectively. Understanding these relationships quantitatively would go a long way in defining the parameter space for which desired morphologies can be achieved (i.e. time/temperature history). Unfortunately, tracking the change in morphology in the gas phase is very difficult to study experimentally, although it can be tracked through MD in a relatively straightforward manner.

Figure 3 shows the temporal behavior during the collision of two 240-atom clusters. The formation of new chemical bonds between the particles results in a decrease in the internal energy as the particle finds a more stable configuration by decreasing its surface area and thus the number of dangling bonds. Since this is an adiabatic problem, the energy release goes into the thermal motion of atoms within the particle and is reflected in a rise in particle
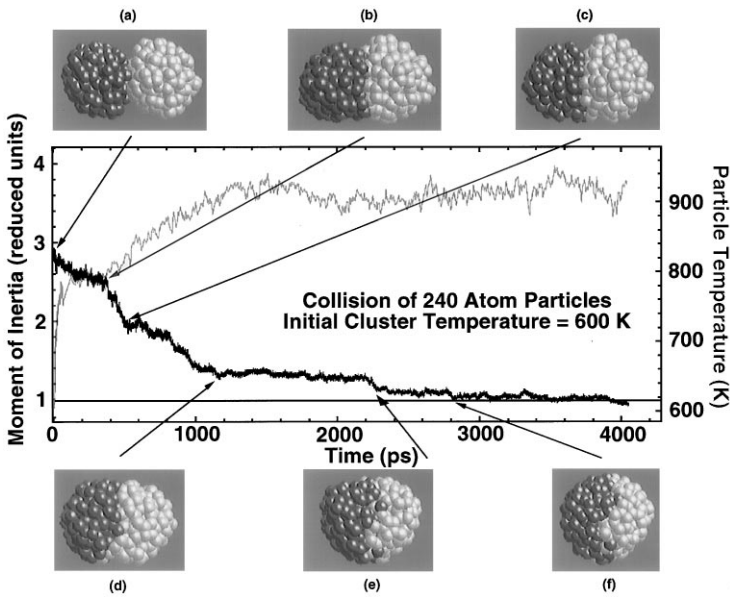
Fig. 3. Temporal behavior of particle morphology as a function of temperature for the collision of two 240-atom particles. The gray curve is temperature. The black curve is the reduced moment of inertia.

temperature. The particle temperature increases by several hundred degrees, such that in a typical growth process the newly formed particles would be significantly hotter than the surrounding gas. It should be noted that the collision energy is a very small fraction of the total energy of the system and is not a factor in the temperature rise observed. Radiative and conductive cooling will eventually lead to a return of the particle's temperature back to that of the ambient environment on a time scale significantly slower than the period of the particle heating. This behavior is in agreement with the shock tube nucleation studies of iron, where black body particle temperatures of 50–150 K higher than the carrier gas were observed (Freund and Bauer, 1977). Figure 3 maps the morphology as a function of time as well as the temperature and reduced moment of inertia in the direction of collision. The reduced moment of inertia along the x-axis converges to unity when the particle becomes perfectly spherical and is used to track the phases of coalescence. Because these are small particles and individual atoms can affect the moment of inertia, a reduced moment of inertia of 1.0 is never really achieved because of the inherent fluctuations in particle shape. For this reason we are using a value of 1.1 to define the attainment of full coalescence. Most of the energy release, as evidenced by the rapid initial temperature rise, occurs when the particles first collide and is caused by the formation of new bonds. This is followed by a more gradual rise in temperature as the resulting agglomerate attempts to coalesce by filling in the "necked" region between the particles. Dumbbell-like structures, formed by neck growth between individual particles in an agglomerate, are often the final result of collisions observed in aerosol processes (see Fig. 2a). The temperature rise continues to the point where neck growth is complete and the particle has an oval shape. Beyond this point the particle shows no discernable change in its internal energy (temperature is constant) as it progresses toward a sphere. Indeed, the time required to become completely spherical, starting from the oval structure, can be as much as half the total sintering time. Qualitatively, this can be thought of as a consequence of the near equivalent stability between an oval and a sphere, which implies a small driving force. The large rapid initial increase in temperature is unique to very small particles due to the fact that the number of new bonds formed at the moment of collision is a larger percentage of the total number of bonds in small particles than in large ones. This phenomenon is displayed in Fig. 4, which shows the initial temperature increase for the collision of various sized clusters. In the present
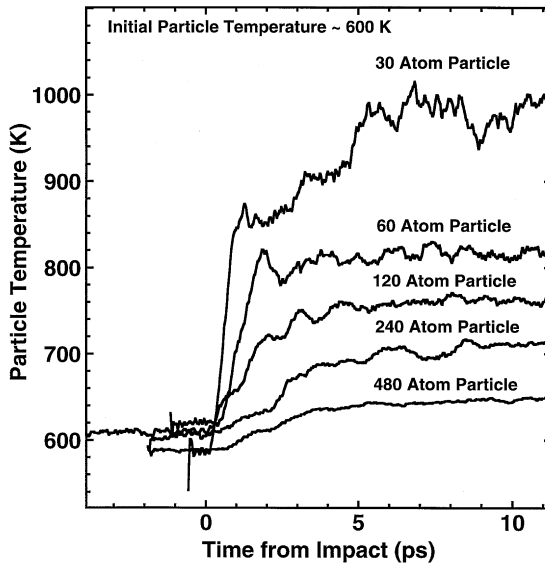
Fig. 4. Temporal evolution of particle temperature showing large initial temperature rise for very small particles.

calculation, due to the fact that there is no buffer gas to remove the energy, the particles will not return to their original temperature. However, since the collisional thermal relaxation with the surrounding bath gas (particle–gas collisions) should be much faster than particle–particle encounters. One should expect that a new particle birth from a particle–particle interaction will increase its temperature, coalesce and then return to its original temperature, prior to an encounter with another particle. For most applications, this is the assumption seen in measurements and modeling of nucleation processes (particle–monomer interactions) which have many analogies to what is taking place here.

To better understand and relate the observed behavior to macroscopic phenomena, we look more closely at the properties of these particles and the nature of the evolution in the morphology. Changes in cluster morphology require the movement of atoms by either bulk fluid motion or by individual atomic diffusional processes. In Fig. 5, we present the temporal evolution of the atomic velocity vectors during a particle–particle collision event. As the clusters approach, the atoms are accelerated toward each other as they feel an attractive force (a). Once the collision event has progressed, atoms move by diffusion to drive the agglomerate to a sphere. Contrary to what one might expect, the coalescence as observed through the atomic motion is not symmetric. As imaged, this case shows that the neck between particles grows by surface diffusion at the "top" of the particles, while interior atoms move down to fill in the neck at the "bottom" (b, c). Prior to initiating these trajectories, care was taken to remove angular momentum from the particles so this behavior is not due to the collision of rotating particles. This asymmetric behavior most likely results, because these particles are never perfect spheres and are always undergoing thermally induced fluctuations. In this particular example, coalescence can be seen to take place from both a surface and a grain boundary mechanism.

The fact that one can track individual atoms with great precision provides significant insights; however, this very atomistic nature also makes it difficult to extract phenomenological mechanisms. An alternative approach is simply to test postulated phenomenological models and determine the quality of the comparison, as described below.

5. EVALUATION OF PHENOMENOLOGICAL MODELS

The driving force for sintering (coalescence) is the minimization of the surface free energy, brought about from a gradient in the chemical potential. While sintering is most generally
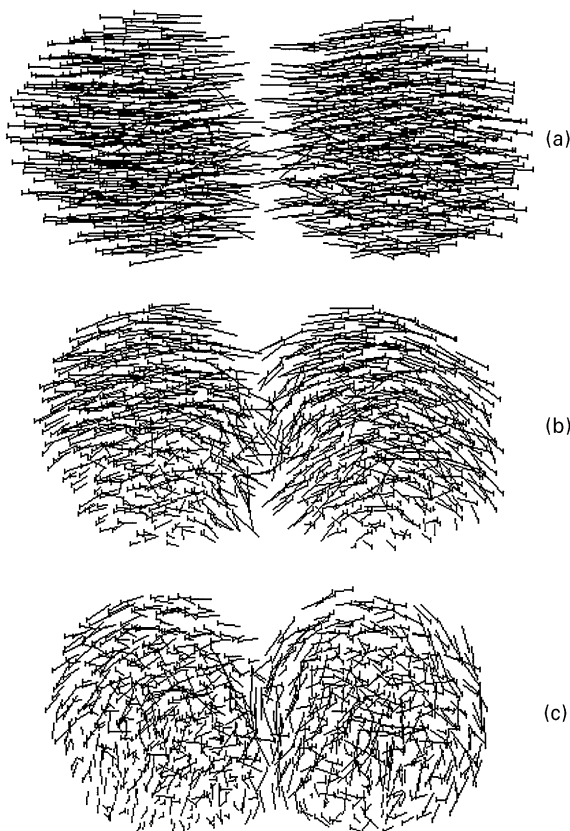
Fig. 5. Time series of particle morphology imaged with respect to atomic velocity vectors for two 480-atom particles at 900 K.

found to be important in the solid-phase (because it is relatively slow), liquid-phase processes can have a large impact on the resulting morphology of multicomponent clusters (Zachariah et al., 1995, 1996b). A number of sintering theories exist that have used phenomenological approaches to describe and provide predictive models. In general, these models employ concepts of viscous flow, diffusion processes and evaporation/condensation as mechanisms for sintering (Kingery and Berg, 1955; Rockland, 1966a, b; Johnson, 1968). Many of these sintering models are based on a derivation for the growth of the neck during the initial sintering process and are not easily extrapolated. A few attempts, however, have been made to model the evolving particle morphology (Nichols and Mullins, 1965; Nichols, 1966).

5.1. Liquid coalescence

For liquid droplets, it is well recognized that the mechanism of coalescence is driven by viscous flow. Both experimental studies (Ryley and Bennett-Cowell, 1967; Ashgriz and Poo, 1990; Jiang et al., 1992) of large droplets as well as continuum formalisms for numerical investigations (Foote, 1973; Lungen and Mansour, 1988; Nobari et al., 1996) have been employed to characterize coalescence. One of the difficulties encountered in these studies, particularly regarding the numerical calculations by continuum means, is dealing with the boundary condition for the interface during collision. For macroscopic drops, the boundary layer of gas surrounding the particles must be displaced in order for a collision to take place. Nanoparticle collision events, however, generally occur in the free molecular regime where one can neglect boundary layer effects. This point will make our computations considerably simpler. Despite these more recent studies, the most useful expression probably comes from

the earliest work in the field by Frenkel (1945), who defined the characteristic coalescence time, τ as

$$\tau = \eta d_p / \sigma, \tag{2}$$

where η is the viscosity, d_p is the particle diameter and σ is the surface tension.

5.2. Solid sintering

For solid particles, the problem is more complex because of the potential for a number of competing transport mechanisms. The extensive number of attempts to model the system is a reflection of the complex geometry being considered which has resulted in a confusing array of coalescence models. These models have been reviewed in the dissertation of Lunden (1995). Lunden also modeled the full geometric evolution of the bi-sphere problem and applied the various sintering rate mechanisms. The conclusions of her work for both silicon and copper were that surface and grain boundary diffusion were the dominant mechanism for solid-like particles and that surface diffusion became more important as the temperature was increased. Experimental data has been sparse, but the situation is changing, albeit primarily for non-oxide systems (Aubert and Canell, 1986; Schmitt-Ott, 1988; Shimada et al., 1994; Seto et al., 1994).

Friedlander and Wu (1994) recently developed a useful expression for the sintering rate of solid-like particles, based on a solid-state diffusion mechanism in which the characteristic coalescence time is represented by the following equation:

$$\tau = \frac{3kTv_p}{64\pi\sigma D(T)v}, \tag{3}$$

where k is Boltzmann's constant, T is the particle initial temperature, v_p is the particle volume, σ is the surface tension, $D(T)$ is the solid-state diffusion coefficient at the particles initial temperature and v is the molecular volume for diffusion. This formulation is based on a linear relationship of the time dependence of the decrease in particle surface area during sintering, in which the driving force is the excess chemical potential due to particle curvature. This basic formalism assumes that both surface and grain boundary diffusion have the same functional dependence. Implementation of this characteristic time requires knowledge of diffusion coefficients and surface tension, both of which can be deduced by molecular dynamics computational methods. In our case, the temperature used was the temperature of the particle a few picoseconds after the collision, as that is the beginning temperature for sintering. The models were designed for large clusters (i.e. 10^6 atoms) which do not have this large initial temperature rise so their sintering begins at the equilibrium temperature. This adjustment enables us to use these models for extremely small particles.

6. EVALUATION OF DIFFUSION COEFFICIENT

Inspection of equation (3) shows that in this formalism the coalescence time should scale as the inverse of the diffusion coefficient, which is very temperature dependent, and proportional to the surface tension. We determined the surface tension of solid particles in a previous study and found them to be relatively insensitive to size (in the regimes of our study). In order to evaluate equation (3), we have computed the diffusion coefficient as a function of temperature, from the initial slope of the atomic mean-square displacement and the Einstein relation (Allen and Tildesey, 1987)

$$D = \frac{1}{6N} \lim_{t \to \infty} \frac{d}{dt} \left\langle \sum_i^N [r_i(t) - r_i(0)]^2 \right\rangle, \tag{4}$$

where N is the number of atoms in the particle and r is the position of each atom. The results of these calculations are presented in Fig. 6 as an Arrhenius plot ($\log D$ vs $1/T$) along with the low-temperature (350–550 K) experimental results of surface diffusion by Mo et al.
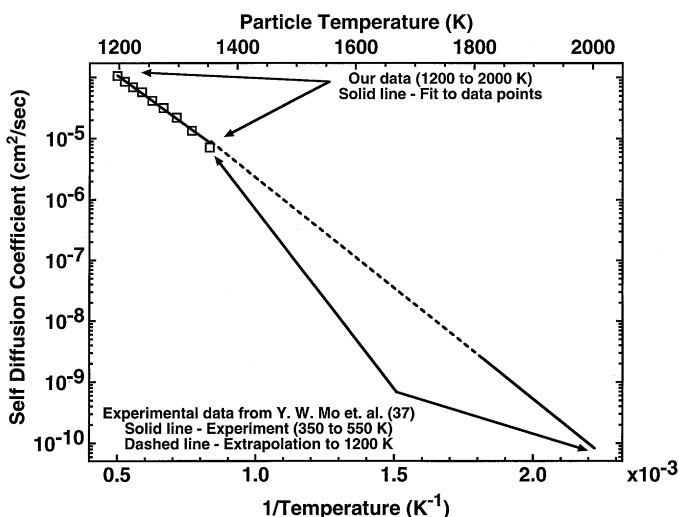
Fig. 6. Computed silicon self-diffusion coefficients. This plot contains our results at high temperatures (1200–2000 K) and the low temperature (350–550 K) experimental data of Mo *et al.* (1992). The dotted line is an extrapolation of Mo's data to 1200 K.

(1992). The computed diffusion coefficients do follow an Arrhenius behavior for the most part, but deviate for the smaller particles at temperatures near the melting point. For this reason, only the 480-atom particles were used in these computations. This deviation from Arrhenius behavior in the diffusion coefficients occurs at temperatures where particle melting/freezing are taking place. The computed melting temperatures are quite broad due to the finite size of the particles. The solid-like particles are actually "glassy" in nature.

This point is illustrated in Fig. 7 which shows the potential energy as a function of temperature. The points were generated by a series of MD computations (with equilibration at each step) in which the cluster energy was monotonically increased (melting curve) or decreased (freezing curve). The change in slope is indicative of a phase transition, although the gradual nature of the change (no discontinuity) indicates the phase transition occurs over a broad range of temperatures. For bulk silicon we expect that the phase change should occur at 1740 K. For nanoparticles, the melting point occurs at significantly lower temperatures (Borel, 1981). For our purposes, these simulations defined the "solid/liquid" boundary, above which we conducted our mean-square displacement calculations for the diffusion coefficients presented above. It is clear from the figure that smaller atoms have a wider temperature range in the melting point, presumably because the surface atoms make up a larger fraction of the mass of the particle. For this reason it is difficult to define an exact melting point for small particles.

The magnitudes of our calculated diffusion coefficients are commensurate with surface diffusion coefficients, as opposed to the known bulk diffusion coefficients for silicon (Mo *et al.*, 1992; Robertson, 1981), implying that these particles behave primarily as surfaces from the point of view of atom mobility. A more complete discussion of the nature of these particles can be found in our earlier work (Zachariah *et al.*, 1996a).

A nonlinear fit to the form of

$$A e^{-B/T} \tag{5}$$

gives an Arrhenius expression of

$$D = 4.69 \times 10^{-3} e^{-7562/T}. \tag{6}$$

This gives an activation energy of 63 kJ mol^{-1} which is in good agreement with the value of 64.7 kJ mol^{-1} obtained by Mo *et al.* (1992) from surface diffusion measurements. However,
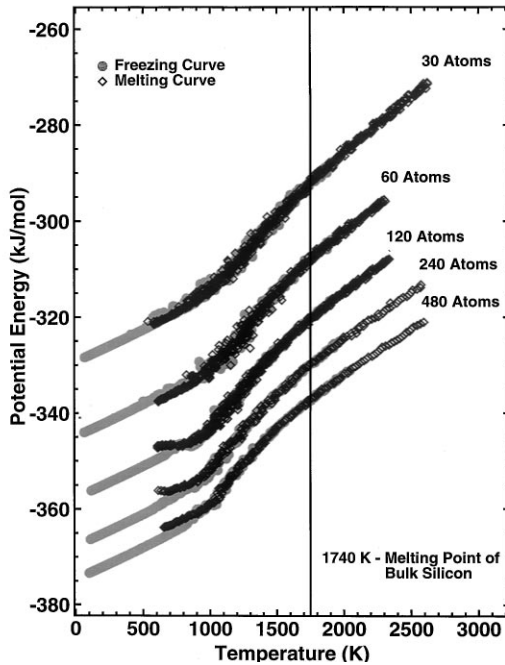
Fig. 7. Freezing and melting point curves as a function of particle size. This shows the range where the particles are all solid, all liquid or a mix of both. The freezing point curve is gray and the melting point curve is black.

we believe that the extent of agreement is probably fortuitous considering the expected accuracy of the SW potential with respect to the silicon binding energy.

The usefulness of the characteristic sintering time τ, once it is determined, comes about because the growth of primary particles by coalescence and the final primary particle size for single-component systems can be estimated using the collision/sintering theory of Koch and Friedlander (1990):

$$\frac{\mathrm{d}a}{\mathrm{d}t} = -\frac{1}{\tau_{\mathrm{f}}}(a - a_{\mathrm{s}}),$$ (7)

where a is the surface area of the coalescing particles, a_{s} is the surface area of a single spherical particle of the same volume, and τ_{f} is the characteristic coalescence time. In the manner of Lehtinen et al. (1996) the variables are changed from particle surface area to particle volume, and can be solved numerically in the form presented, or alternatively incorporated within the framework of the general dynamic equations for aerosol growth. Naturally, the accuracy and ultimate utility of the results are very much dependent upon the functional form of the characteristic times as well as the availability and accuracy of the fundamental thermophysical property data needed for their evaluation. Indeed, one of the great frustrations in this area is the lack of property data at the dimensions involved and the sparse nature of the sintering results available for isolated particle growth. Fortunately, the reasons (i.e. small scale) that make experiments so difficult, make molecular level computations feasible and an attractive alternative to probe the structure, energetics and kinetics of nanoscale materials.

7. TRAJECTORY CALCULATIONS: COMPARISON WITH PHENOMENOLOGICAL MODELS

Several trajectories have been computed as a function of size and temperature to define the dependence of these variables on the coalescence time. The results of these calculations
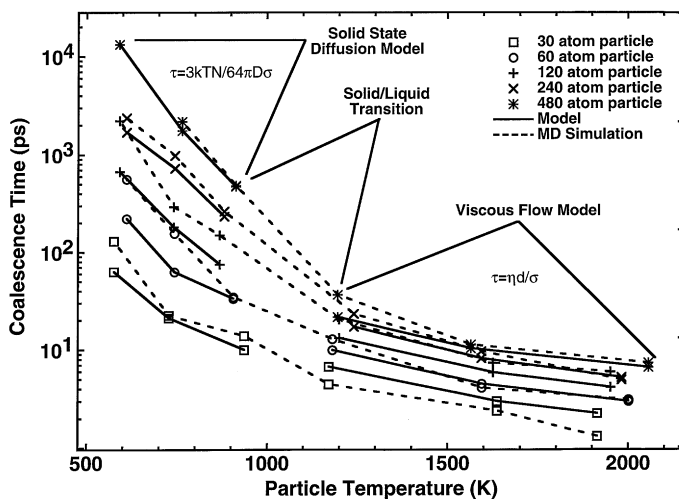
Fig. 8. Coalescence times as a function of particle size and temperature. Dotted lines connect the MD computations. The solid curves represent the viscous and solid state diffusion models. Note: The model results for the liquid phase were increased by a factor of ten so they would line up with the MD simulations.

are presented in Fig. 8. Several general features are readily apparent. At the higher temperatures, when the particles are clearly in the liquid state, the dependence of size and temperature on coalescence is small. At the lowest temperatures, when the particles are clearly solid-like, the dependence of size and temperature on coalescence is quite strong, and cluster coalescence rates are sufficiently long as to make the coldest and largest particle (600 K, 480 atoms) computationally intractable. Notice that the results are presented on a semi-log plot.

Also presented in the figure is a comparison with the liquid and solid coalescence models discussed above. For the solid particles, the transport properties employed in the phenomenological model are those computed from the MD calculations, making the comparison between the MD and phenomenological models for the solid particles self-consistent. We believe these to be the first comparisons of a full atomistic model with phenomenological models for particle sintering. For the liquid particles the data for the surface tension and viscosity was obtained from experimental results (Yaws *et al.*, 1981) since these properties change over the temperature range we are using. The results for the liquid clusters needed to be multiplied by a factor of 10 to overlay them with the results of the MD calculations. The underprediction of the coalescence time is presumably due to our use of viscosity data for bulk silicon which is not as accurate for very small particles. However, the general trend of the scaled results of the model matches quite well with the MD simulation, particularly the size dependence.

Our primary interest is the coalescence time of solid-like clusters, since this region ultimately traps the morphology into an agglomerate. In this region, we see a very strong dependence on both particle size and temperature. The strong dependence on temperature correlates very well with the temperature dependence in the diffusion coefficient. Indeed, application of the solid-state diffusion model (equation (3)) gives quantitative agreement between the model and the MD computations. The model does an excellent job of predicting both the severe temperature and size dependence of the sintering rate. The validation of this mechanism of sintering implies that the availability of property data should enable a quantitative prediction of the characteristic sintering time which can be implemented within the framework of existing aerosol growth models.

In summary, both the MD computation and the sintering models show a strong dependence on particle size for the colder, solid-like clusters ($\propto d^3$) and a weaker dependence when liquid-like ($\propto d$). There is a region in which neither model is applicable, which

corresponds to particle solidification/melting as determined by computation of the potential energy dependence on temperature (Fig. 7). Because of the finite nature of these particles, they do not undergo a first-order phase transition but have a wide band in temperature over which melting/solidification takes place. Nevertheless, in the limit where these particles are either all solid or all liquid, the comparison between the phenomenological and atomistic models is excellent.

8. CONCLUSIONS

Molecular dynamics trajectory calculations were conducted to obtain the kinetics of growth and sintering of silicon nanoparticles. Calculations were conducted with up to 1000-atoms which corresponded to a 3 nm diameter particle. Sintering effects have shown that particle morphology is very sensitive to temperature as is the coalescence time. The coalescence time was also shown to be very sensitive to particle size for solid-like particles and relatively independent of cluster size for molten particles. The results have for the first time validated phenomenological sintering models using a molecular-based model. In particular, the results show that a solid-state diffusion model quantitatively predicts the sintering time.

REFERENCES

Allen, M. P. and Tildesley, D. J. (1987) *Computer Simulation of Liquids*. Oxford Science Press, Oxford.

Ashgriz, N. and Poo, J. Y. (1990) Coalescence and separation in binary collisions of liquid-drops. *J. Fluid. Mech.* **221,** 183–204.

Aubert, C. and Cannell, D. S. (1986) Restructuring of colloidal silica aggregates. *Phys. Rev. Lett.* **56,** 738–741.

Blasiten-Barojas, E. and Zachariah, M. R. (1992) Molecular-dynamics study of cluster growth by cluster–cluster collisions. *Phys. Rev. B* **45,** 4403–4408.

Borel, J.-P. (1981) Thermodynamical size effect and the structure of metallic clusters. *Surf. Sci.* **106,** 1–9.

Foote, G. B. (1973) A numerical method for studying liquid drop behavior: simple oscillation. *J. Comput. Phys.* **11,** 507–530.

Frenkel, J. (1945) Viscous flow of crystalline bodies under the action of surface tension. *J. Phys.* **9,** 385–391.

Friedlander, S. K. and Wu, M. K. (1994) Linear rate law for the decay of the excess surface-area of a coalescing solid particle. *Phys. Rev. B* **49,** 3622–3624.

Freund, H. J. and Bauer, S. H. (1977) Homogeneous nucleation in metal vapors. 2. Dependence of the heat of condensation on cluster size. *J. Phys. Chem.* **81,** 994–1000.

Gay, J. G. and Berne, B. J. (1986) Energy accommodation in collisions of small particles. *J. Colloid Interface Sci.* **109,** 90–100.

German, R. M. (1996) *Sintering Theory and Practice*. Wiley, New York.

Girshick, S., Rao, N., Haberlein, J., McMurry, P., Jones, S., Hansen, D. and Micheel, B. (1995) Nanoparticle formation using a plasma expansion process. *Plasma Chem. Plasma Process.* **15,** 581–607.

Jiang, Y. J., Umemura, A. and Law, C. K. (1992) An experimental investigation on the collision behavior of hydrocarbon droplets. *J. Fluid Mech.* **234,** 171–190.

Johnson, D. L. (1968) New method of obtaining volume, grain-boundary, and surface diffusion coefficients from sintering data. *J. Appl. Phys.* **40,** 192–200.

Kingery, W. D. and Berg, M. (1955) Study of the initial stages of sintering solids by viscous flow, evaporation–condensation, and self-diffusion. *J. Appl. Phys.* **26,** 1205–1212.

Koch, W. and Friedlander, S. K. (1990) The effect of particle coalescence on the surface-area of a coagulating aerosol. *J. Colloid Interface Sci.* **140,** 419–427.

Lehtinen, K. E. J., Windeler, R. S., Friedlander, S. K. (1996) A note on the growth of primary particles in agglomerate structures by coalescene. *J. Colloid Interface Sci.* **182,** 606–608.

Lunden, M. M. (1995) Sintering of aerosol agglomerates. Ph.D. dissertation, California Institute of Technology, Pasadena, CA.

Lundgren, T. S. and Mansour, N. N. (1988) Oscillations of drops in zero gravity with weak viscous effects. *J. Fluid. Mech.* **194,** 479–510.

Mo, Y.-W., Kleiner, J., Webb, M. B. and Lagally, M. G. (1992) Surface self-diffusion of Si on Si(001). *Surface Science* **268,** 275–295.

Nichols, F. A. and Mullins, W. W. (1965) Morphological changes of a surface of revolution due to capillarity-induced surface diffusion. *J. Appl. Phys.* **36,** 1826–1835.

Nichols, F. A. (1966) Coalescence of two spheres by surface diffusion. *J. Appl. Phys.* **37,** 2805–2808.

Nobari, M. R., Jan, Y-J. and Tyggvason, G. (1996) Head on collision of drops. *Phys. Fluids.* **8,** 29–42.

Robertson, W. M. (1981) Thermal etching and grain-boundary grooving of silicon ceramics. *J. Am. Ceram. Soc.* **64,** 9–13.

Rockland, J. G. R. (1966) On the rate equation for sintering by surface diffusion. *Acta Metallurgica* **14,** 1273–1279.

Rockland, J. G. R. (1967) The determination of the mechanism of sintering. *Acta Metallurgica.* **15,** 277–286.

Ryley, D. J. and Bennett-Cowell, B. N. (1967) The collision behavior of steam-borne water drops. *Int. J. Mech. Sci.* **9,** 817–833.

Schmitt-Ott, A. (1988) In situ measurement of the fractal dimensionality of ultrafine aerosol particles. *Appl. Phys. Lett.* **52,** 954–956.

Seto, T., Shimada, M. and Okuyama, K. (1995) Evaluation of sintering of nanometer-sized titania using aerosol method. *Aerosol Sci. Technol.* **23,** 183–200.

Shimada, M., Seto, T. and Okuyama, K. (1994) Size change of very fine silver agglomerates by sintering in a heated flow. *J. Chem. Engng Japan* **27,** 795–802.

Siegel, R. W. (1994) In *Nanophase Materials*: *Synthesis*, *Structure and Properties* (Edited by Fujita, F. E.), Springer Series in Materials Science, Vol. 27. Springer, Berlin.

Stillinger, F. H. and Weber, T. S. (1985) Computer simulation of local order in condensed phases of silicon. *Phys. Rev. B.* **31,** 5262–5271.

Xiong, Y., Akhtar, M. K. and Pratsinis, S. E. (1993) Formation of agglomerate particles by coagulation and sintering. 2. The evolution of the morphology of aerosol-made titania, silica, and silica doped titania powders. *J. Aerosol Sci.* **24,** 301–313.

Yaws, C. L., Dickens, L. L., Lutwack, R. and Hsu, G. (1981) Semiconductor industry silicon: physical and thermodynamic properties. *Solid State Technol.* **24,** 87–92.

Zachariah, M. R., Carrier, M. J. and Blaisten-Barojas, E. (1994) Molecular dynamics simulation of large cluster growth. In *Gas-Phase and Surface Chemistry in Electronic Materials Processing*, MRS, Proceedings (Edited by T. J. Mountziaris), Vol. 334, pp. 75–80.

Zachariah, M. R., Aquino-Class, M., Shull, R. D. and Steel, E. (1995) Formation of superparamagnetic nanocomposites from vapor phase condensation in a flame. *Nanostructured Mater.* **5,** 383–392.

Zachariah, M. R., Carrier, M. J. and Blaisten-Barojas, E. (1996a) Properties of silicon nanoparticles: a molecular dynamics study. *J. Phys. Chem.* **100,** 14856–14864.

Zachariah, M. R., Shull, R. D., McMillin, B. K. and Biswas, P. (1996b) In situ characterization and modeling of the vapor-phase formation of a magnetic nanocomposite *Nanotechnology*: *Molecularly Designed Materials* (Edited by Chow, G. and Gonsalves, K.), ACS Series, Vol. 622, Chap. 3, pp. 42–64. American Chemical Society, Washington, DC.

Zhu, H. L. and Averback, R. S. (1996a) Sintering of nano-particle powders: simulations and experiments. *Mater. Manufacturing Proc.* **11,** 905–923.

Zhu, H. L. and Averback, R. S. (1996b) Sintering processes of two nanoparticles: a study by molecular dynamics simulations. *Philos. Mag. Lett.* **73,** 27–33.